

Supplementary Material

Direct fabrication of high-quality vertical graphene nanowalls on arbitrary substrates without catalysts for tidal power generation

Junkui Zhu,^a Honglie Shen,^{*a} Zehui Wang,^a Yufang Li,^a Tianru Wu,^b Weibiao Mao,^a

and Jingzhe Zhang^a

^a. Address here Jiangsu Key Laboratory of Materials and Technology for Energy Conversion, College of Materials Science & Technology, Nanjing University of Aeronautics & Astronautics, Nanjing 210016, China

^b. State Key Laboratory of Functional Materials for Informatics Shanghai Institute of Microsystem and Information Technology, Chinese Academy of Sciences, Shanghai 200050, China

1) The process for depositing vertical graphene nanowalls (VGN).

In the deposition process of HWCVD to prepare VGN, the experimental parameters and duration of each stage were shown in Fig. S1.

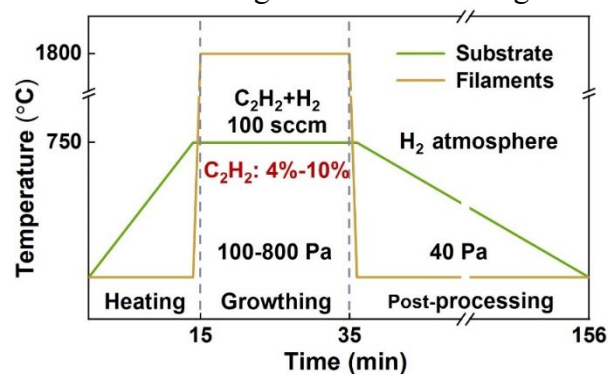


Fig. S1 The deposition process of the HWCVD method for depositing the VGN layer.

2) The distance from the filament to the substrate.

At proper pressure, the C₂H* group had a proper mean free path, which was just the same as the distance from the filament to the surface of the substrate, as shown in Fig. S2. It was conducive to the selection of carbon active groups.

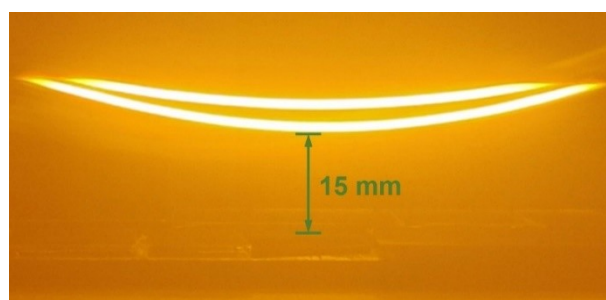
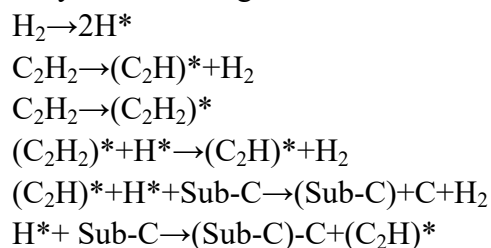


Fig. S2 Schematic diagram of the distance from the filament to the substrate surface.

3) Reasons for using acetylene as a precursor for VGN growth and its reaction process.

The choice of C_2H_2 was necessary to obtain a high-quality VGN at a substrate temperature of 750 °C. On the one hand, the C-H bonds of various precursor carbon sources have different fracture capacities. The use of precursors with low C-H bond energy in the CVD process of VGN could reduce the amount of energy absorbed during the pyrolysis of the carbon source and inhibit the recombination of carbon active groups during mass transfer, which was necessary to achieve the growth of VGN at lower substrate temperature. The dehydrogenation ability of hydrocarbons was the key factor affecting the synthesis temperature of graphene. When CH_4 was used as a precursor, the reaction temperature should reach 900 °C, otherwise, the precursor could not be cracked¹. In this work, the substrate temperature should be controlled at 750 °C. Under these conditions, the decomposition CH_4 was easy to compound in the mass transfer and the graphene could not grow. According to the above, C_2H_2 , which requires less energy for cracking and lower temperature for cleavage, was selected as the precursor to achieve the substrate temperature controlled at about 400-850°C during the preparation of VGN.

On the other hand, compared with precursors such as CH_4 and C_2H_6 composed of C-C bonds, $C\equiv C$ in C_2H_2 was more likely to form $(C_2H_2)^*$ and $(C_2H)^*$ active clusters after cracking, which was conducive to the formation of carbon hexagon rings². The less H content of C_2H_2 made the H^* produced by the cracking of the H_2 in reaction gas easier to peel off the H on the C Group. The reaction of graphene growth on the substrate could be described by the following reaction formula³:



The amorphous carbon and SP^3 hybrid carbon could be effectively etched when H_2 was used as the auxiliary gas in the precursor gas. Therefore, the appropriate $C_2H_2:H_2$ ratio could significantly improve the crystallization quality of VGN.

4) Analysis of the influence of the substrate temperature (T_{sub}) during the preparation process on the morphology and crystal quality of VGN.

In addition to air pressure, T_{sub} was also an important factor affecting the morphology and quality of VGN. The T_{sub} determined the number of initial nucleation, as well as the form of carbon group agglomeration, dehydrogenation rate, growth rate, and so on. It was found that high temperature was beneficial to accelerating the growth of VGN, as the SEM cross-sections shown in Figures S3(a) and S3(b). With a growth time of 30 minutes, the thickness of VGN could reach 358.2 nm at a T_{sub} of 400 °C. If the temperature was increased to 850 °C it could reach 734.4 nm almost twice the former, while the density of VGN nanosheets at 400 °C

was significantly higher than that at 800 °C. The SEM cross-sectional view of growth at different T_{sub} (Figure S3(c)) showed that at a high temperature, nanosheets were more inclined to grow vertically and anisotropically, with a larger sheet area and better verticality. After the temperature dropped to 400 °C, the nanosheets began to grow isotropically with the disorder arrangement and lots of edges, which was also one of the reasons for the degradation of the Raman characteristics.

Due to the fast growth rate of the HWCVD method⁷, according to Fick's law of diffusion⁵, the precursor had a strong ability to diffuse on the substrate surface at a high temperature. Therefore, the probability of aggregate growth was much lower than that under low-temperature conditions, which caused the nucleation density at low temperatures to be much higher than that at high temperatures. At a high temperature, since the active groups of the precursor were not easy to recombine, the concentration of reaction precursors that could participate in the growth was higher. And the high temperature also could improve the diffusion growth ability of the precursor, thereby achieving rapid growth at high temperature and low density. Besides, a high temperature also improved the quality of VGN. As could be seen in Figure S3(e), the higher the temperature, the more obvious the 2D peak, and the lower and lower half-height width of the 2D peak indicating that the crystalline quality had also improved with the increase in temperature. Figure S3(f) further analyzed the result of Raman. The I_D/I_G value got lower and lower as the temperature increased while the value of I_{2D}/I_G increased and stabilized at 750°C. This was because the high temperature reduced the recombination probability of H^* . The content of H^* which could etch the VGN was positively correlated with temperature. At a high temperature, H^* had a very strong etch effect on sp^3 phases and amorphous carbon, which was reflected in the reduction of the defect density of VGN at this temperature.

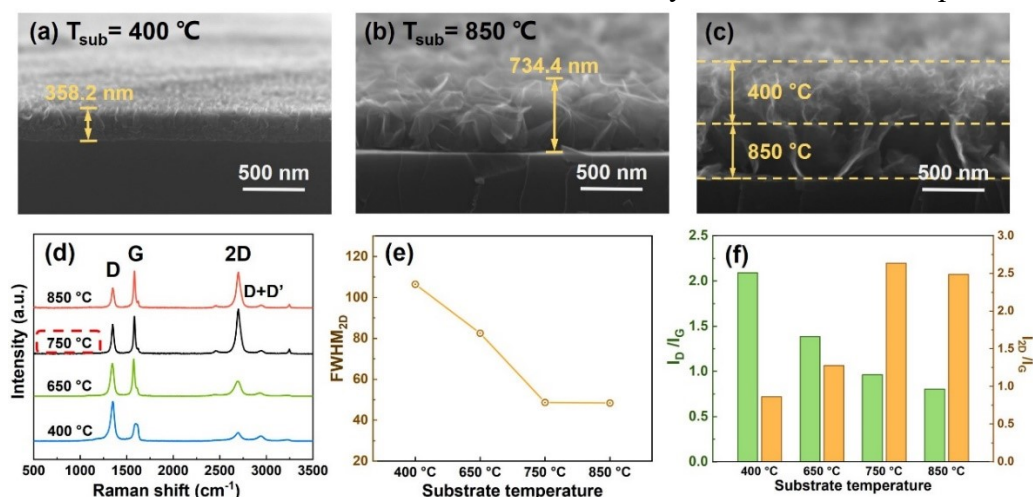


Fig. S3 The regulating effect of temperature on the morphology and quality of VGN (c-Si substrate): (a) SEM cross-sections of VGN at 400 °C. (b) SEM cross-sections of VGN at 850 °C. (c) SEM cross-sections of VGN at a changing T_{sub} . (d) Raman spectra of VGN at different temperature conditions. (e) The FWHMD change curve at different temperature conditions. (f) Comparison of I_D/I_G and I_{2D}/I_G values of VGN Raman curve at different temperature conditions.

5) Analysis of the influence of the C₂H₂ partial pressure during the preparation process on the morphology and crystal quality of VGN.

We also analyzed the influence of the C₂H₂ partial pressure on the quality of graphene. A too low ratio of C₂H₂ would not be able to form graphene due to insufficient carbon sources, while a too high ratio of H₂ would have an inhibitory effect on the cracking of C₂H₂. But an excessively high proportion of C₂H₂ would result in a rapid increase in the content of amorphous carbon⁶. As shown in Figure S4(b), an excessively high C₂H₂ concentration would cause the nanowall structure to almost disappear, showing a tendency to transform into a graphite-like structure. This was mainly because at a suitable H₂ concentration and under the condition of ensuring the supply of C₂H*, a higher H₂ ratio could inhibit the occurrence of graphene defects. If H₂ was insufficient, a large number of C=C chains, such as olefins, would appear in graphene without forming a conjugated hexagonal structure and accompanied by the production of a large amount of amorphous carbon, which leads to serious graphene crystal quality reduction.

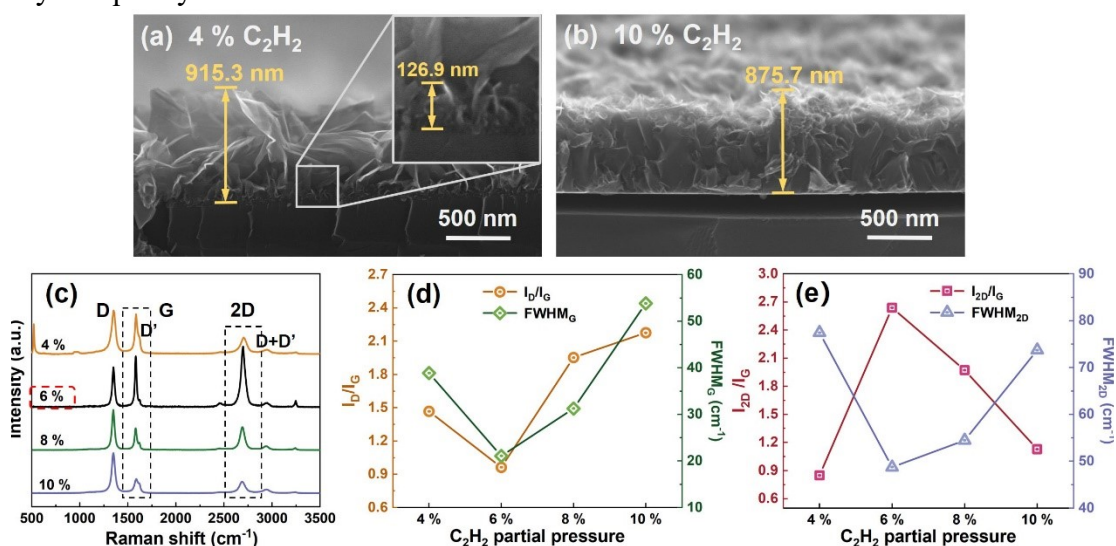


Fig. S4 The regulating effect of C₂H₂ partial pressure on the morphology and quality of VGN: (a-b) SEM cross-sectional view of VGN at the condition of partial pressure of 4% and 10%. (c) Raman spectra of VGN at different C₂H₂ partial pressure. (d) The change curve of I_D/I_G intensity and FWHM_G at different C₂H₂ partial pressure. (e) The change curve of I_{2D}/I_G intensity and FWHM_{2D} at different C₂H₂ partial pressure.

6) The good conformal properties of VGN.

The HWCVD direct growth method to prepare VGN was conducive to making them able to fully adhere to the complex substrate surface.

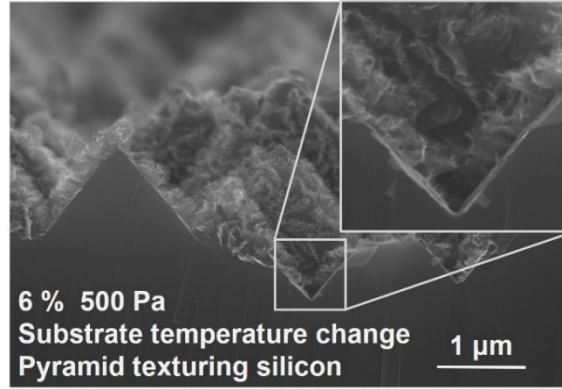


Fig. S5 VGN deposited on pyramid-textured c-Si substrates with good conformal properties.

7) The excellent stability and repeatability of output current and voltage.

VGN hydrovoltaic power generation devices prepared at various conditions all showed high stability and repeatability of output current and voltage.

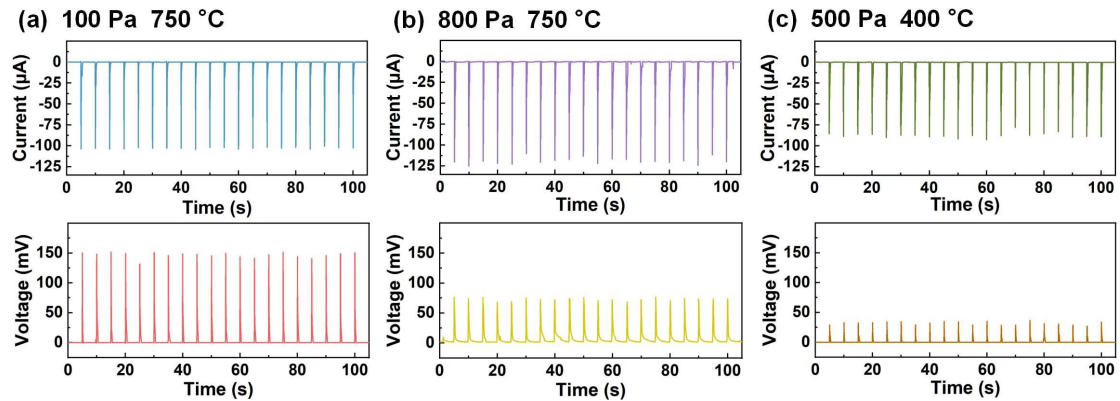


Fig. S6 The output current and voltage signals of the device prepared at the different VGN deposition parameters within 20 cycles (C_2H_2 partial pressure were all at 6 %): (a) Pressure 100 Pa, T_{sub} 750 °C. (b) Pressure 800 Pa, T_{sub} 750 °C. (c) Pressure 500 Pa, T_{sub} 400 °C.

8) The main principle of the droplet-type hydrovoltaic power generation device

The anions within the NaCl droplets adsorb positively charged holes in the VGN in contact with the droplets. With the action of Coulomb force, an electric double layer was formed at the interface, thereby forming a pseudocapacitive structure inside the droplet. As the droplet slid along the device, the Cl^- anions in the droplet migrated toward the direction of the droplet movement, and the holes in the VGN were attracted and aggregated. The charge migration brought about by this movement caused the pseudocapacitive at the front of the droplet to continuously charge and the back end to discharge continuously, forming a potential difference and resulting in induced voltage and current^{7, 8}.

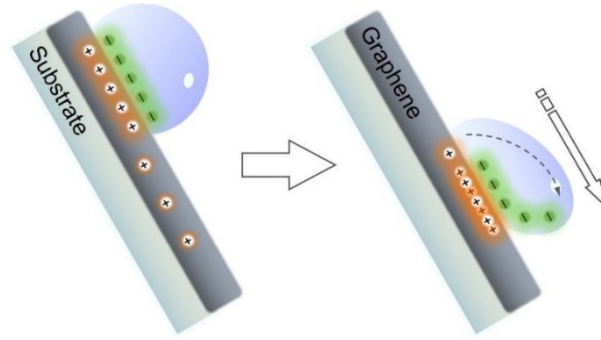


Fig. S7 Principle schematic diagram of droplet type hydrovoltaic power generation device

9) Analysis of hydrophobicity of VGN.

VGN had good hydrophobicity and could significantly increase the contact angle of the quartz glass surface. The decrease in the crystal quality of VGN would lead to a decrease of their hydrophobicity.

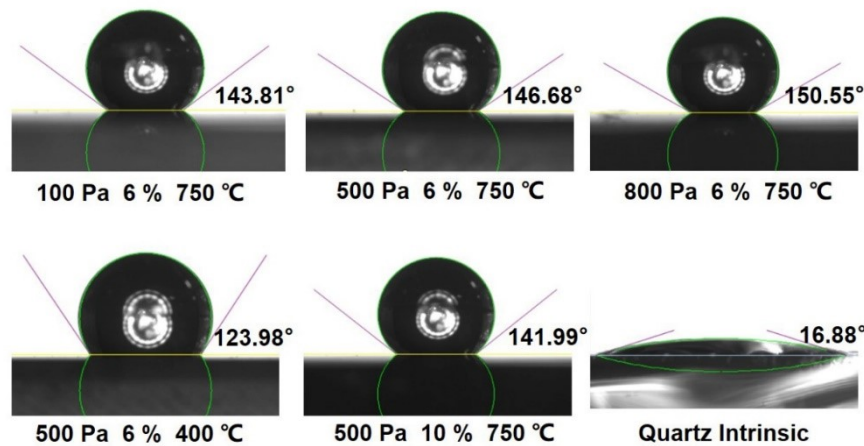


Fig. S8 The contact angle of VGN prepared on quartz glass at different deposition conditions and the intrinsic contact angle of quartz glass.

10) Effect of VGN height on device power.

The height of the graphene nanowall could affect the output power of the device. Generally higher height of nanowall meant a larger domain area. We found that the area of graphene nanosheets was larger when the deposition pressure was 100 Pa, which meant a larger contact area with the droplet (Fig.S9 (a) and (b)). As the deposition pressure increased, the perpendicular degree of the domains increased and the area decreased, resulting in the contact between the graphene nanosheet and the droplet changing from surface contact to edge contact. The reduction in the contact area resulted in a reduction in the area that could form a double-layer structure. This resulted in the formation of a pseudocapacitor structure with a decrease in the value of C_0 . The output current I tended to decrease with the decrease of nanowall height, which depended on the pressure of the sediment. (Fig.S9. (c))

In addition, graphene nanowall with low height and good verticality was an excellent hydrophobic structure. This was not ideal for the capacitance of the pseudocapacitor. Therefore, it was considered that the higher height of the graphene domain, which could lodge to provide greater contact, was beneficial to increasing the output power of the device.

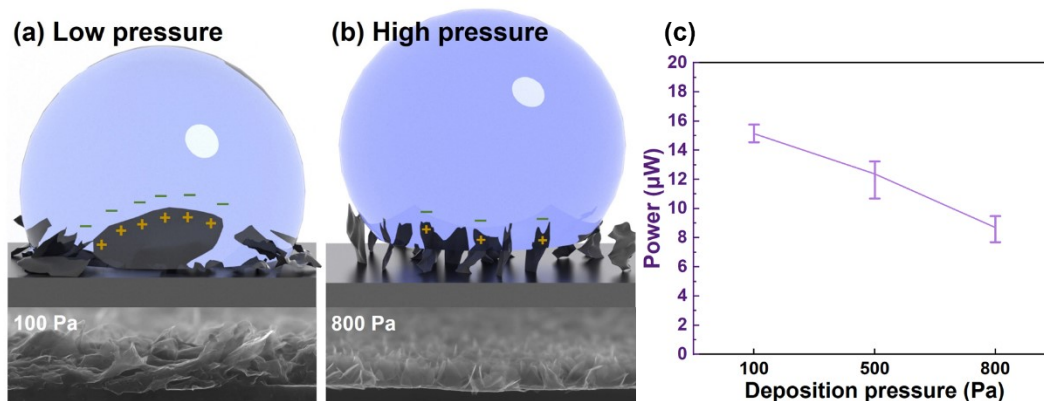


Fig.S9 Effect of graphene nanowalls height on device output power: (a) Contact mode at low pressure. (b) Contact mode at high pressure. (c) The output power of VGN hydrovoltaic generation devices prepared at different pressure conditions.

11) The influence of T_{sub} on the square resistance (R_S).

The deterioration of the conductivity of VGN, which was caused by the decrease of T_{sub} , reduced the output current.

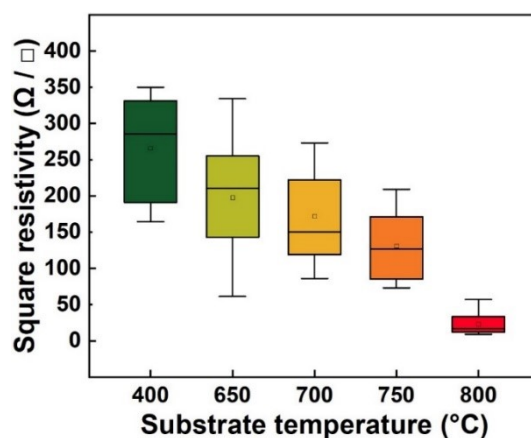


Fig. S10 Fluctuation interval of R_S of VGN film prepared at different T_{sub} and their change trend.

Notes and references

- 1 J.-b. Wang, Z. Ren, Y. Hou, X.-l. Yan, P.-z. Liu, H. Zhang, H.-x. Zhang and J.-j. Guo, *New Carbon Mater.*, 2020, **35**, 193-208.
- 2 H. Oberg, Y. Nestsarenka, A. Matsuda, J. Gladh, T. Hansson, L. G. Pettersson and H. Ostrom, *The Journal of Physical Chemistry C*, 2012, **116**, 9550-9560.
- 3 M. Qi, Z. Ren, Y. Jiao, Y. Zhou, X. Xu, W. Li, J. Li, X. Zheng and J. Bai, *The Journal of Physical Chemistry C*, 2013, **117**, 14348-14353.
- 4 R. Schropp, *Thin Solid Films*, 2009, **517**, 3415-3419.

- 5 H. J. Park, J. Meyer, S. Roth and V. Skákalová, *Carbon*, 2010, **48**, 1088-1094.
- 6 Z. Zhai, H. Shen, J. Chen, X. Li and Y. Jiang, *J. Mater. Chem. A*, 2019, **7**, 12038-12049.
- 7 H. Cai, Y. Guo and W. Guo, *Nano Energy*, 2021, **84**, 105939.
- 8 Z. Zhang, X. Li, J. Yin, Y. Xu, W. Fei, M. Xue, Q. Wang, J. Zhou and W. Guo, *Nat Nanotechnol*, 2018, **13**, 1109-1119.